C_{30} Self-Assembled Monolayers on Silica, Titania, and Zirconia: HPLC Performance, Atomic Force Microscopy, Ellipsometry, and NMR Studies of Molecular Dynamics and Uniformity of Coverage

Matthias Pursch,*,† David L. Vanderhart,‡ Lane C. Sander,† Xiaohong Gu,§ Tinh Nguyen,§ Stephen A. Wise,† and Donald A. Gajewski||

Contribution from the Analytical Chemistry Division, Chemical Science and Technology Laboratory, Polymers Division, Materials Science and Engineering Laboratory, Building Materials Division, Building and Fire Research Laboratory, and Semiconductor Electronics Division, Electronics and Electrical Engineering Laboratory, National Institute of Standards and Technology (NIST), Gaithersburg, Maryland 20899

Received October 15, 1999. Revised Manuscript Received May 2, 2000

Abstract: C_{30} self-assembled monolayers (SAMs) have been prepared on zirconia, titania, and two different silica gels by reacting C_{30} trichlorosilane with the humidified surfaces. ^{13}C solid-state NMR spectroscopy indicated higher alkyl chain order on titania and zirconia materials than on the silica C_{30} phases. Order is inferred from the relative intensity of the main methylene carbon resonance assigned to an all-trans conformation. Carbon longitudinal relaxation time (T_1^C) data reveal that these ordered alkyl chains still have large-amplitude motions on submicrosecond time scales at ambient temperature. Since fast diffusional rotation about the chain axis is compatible with an all-trans conformation, T_1^C, carbon chemical shift, and proton line width data for the alkane rotator phase (C_{19}) and the C_{30} phases were compared. Proton spin diffusion experiments were also conducted using an initial polarization gradient based on mobility differences. These experiments indicated both a higher mobility for the free end of the immobilized chains and heterogeneity in the density of coverage on at least the 20-nm distance scale. The methyl carbon line shape is also discussed in detail since its chemical shift conveys information about both mobility and interactions with an air interface in a dry sample. Atomic force microscopy and contact angle studies indicated a greater surface roughness for C_{30} SAMs compared to C_{18} SAMs prepared on silicon. Ellipsometry revealed film thicknesses of 2.82 nm for the C_{18} SAM and 4.05 nm for the C_{30} SAM. High shape selectivity was found in correspondent liquid chromatographic (LC) separations of polycyclic aromatic hydrocarbons, carotenoids, and tocopherols. The LC data confirm the highly organized alkyl chain arrangement on zirconia and titania, which provide an alternative to the silica-based reversed phases.

Introduction

Self-assembled monolayers (SAMs) are receiving widespread and increasing interest in materials research.[1−5] The majority of monolayers are formed by reaction of sulfur-containing ligands with transition metal (gold, silver, copper) surfaces. A thoroughly described example is the SAM formation of alkanethiols on gold surfaces.[2] SAMs are also easily prepared by silanization of silicon surfaces. Most of these studies described formation, structure, and dynamics of a wide variety of C_{18} SAMs. Very few long-chain (C_{30}) SAMs have been reported so far.[6−8]

Silica gel-based C_{30} phases designed for liquid chromatography (LC) have received increased attention after their development for carotenoid separations by Sander et al.[9] Applications have included separations of carotenoid [9−14] and vitamin A isomers,[15] fullerenes,[16] tocopherols,[17] and tocotrienols.[18] These

* Current address: Dow Deutschland Inc., Industriestr. 1, 77836 Rheinmuenster, Germany. E-mail: MPursch@dow.com.

† Analytical Chemistry Division, Chemical Science and Technology Laboratory.

‡ Polymers Division, Materials Science and Engineering Laboratory.

§ Building Materials Division, Building and Fire Research Laboratory.

|| Semiconductor Electronics Division, Electronics and Electrical Engineering Laboratory.

(1) Nuzzo, R. G.; Allara, D. L. *J. Am. Chem. Soc.* **1983**, *105*, 4481−4483.

(2) Ulman, A. *Chem. Rev.* **1996**, *96*, 1533−1554.

(3) Wasserman, S. R.; Whitesides, G. M.; Tidswell, I. M.; Ocko, B. M.; Pershan, P. S.; Axe, J. D. *J. Am. Chem. Soc.* **1989**, *111*, 5852−5861.

(4) Maoz, R.; Sagiv, J. *J. Colloid Interface Sci.* **1984**, *100*, 465.

(5) Badia, A.; Gao, W.; Singh, S.; Demers, L.; Cuccia, L.; Reven, L. *Langmuir* **1996**, *12*, 1262−1269.

(6) Boehm, C.; Leveiller, F.; Moehwald, H.; Kjaer, K.; Als-Nielsen, J.; Weissnuch, I.; Leiserowitz, L. *Langmuir* **1994**, *10*, 830−836.

(7) Bierbaum, K.; Grunze, M.; Baksi, A. A.; Chi, L. F.; Schrepp, W.; Fuchs, H. *Langmuir* **1995**, *11*, 2143-2150.

(8) Bierbaum, K.; Kinzler, M.; Woell, C. H.; Grunze, M.; Haehner, G.; Heid, S.; Effenberger, F. *Langmuir* **1995**, *11*, 512−518.

(9) Sander, L. C.; Sharpless, K. E.; Craft, N. E.; Wise, S. A. *Anal. Chem.* **1994**, *66*, 1667−1674.

(10) Emenhiser, C.; Sander, L. C.; Schwartz, S. J. *J. Chromatogr.* **1995**, *707*, 205−216.

(11) Emenhiser, C.; Englert, G. E.; Sander, L. C.; Ludwig, B.; Schwartz, S. *J. Chromatogr., A* **1996**, *719*, 333−343.

(12) Strohschein, S.; Pursch, M.; Haendel, H.; Albert, K. *Fresenius' J. Anal. Chem.* **1997**, *357*, 4498−502.

(13) Delgado-Vargas, F.; Paredes-Lopez, O. *J. Agric. Food Chem.* **1997**, *45*, 1097−1102.

(14) Dachtler, M.; Kohler, K.; Albert, K. *J. Chromatogr., B* **1998**, *720*, 211−216.

(15) Strohschein, S.; Schlotterbeck, G.; Richter, J.; Pursch, M.; Tseng, L. H.; Haendel, H.; Albert, K. *J. Chromatogr., A* **1997**, *765*, 207−214.

(16) Ohta, H.; Jinno, K.; Saito, Y.; Fetzer, J. C.; Biggs, W. R.; Pesek, J. J.; Matyska, M. T.; Chen, Y. L. *Chromatographia* **1996**, *42*, 56−62.

(17) Strohschein, S.; Pursch, M.; Lubda, D.; Albert, K. *Anal. Chem.* **1998**, *70*, 13−18.

10.1021/ja993705d
Published on Web 07/08/2000

studies have demonstrated that the high degree of molecular shape recognition for structural isomers is characteristic of polymeric C_{30} phases.[19] Polymeric C_{30} phases can be prepared by solution polymerization of the corresponding trichlorosilane when water is added to the silica slurry. Solid-state NMR studies confirmed that the alkyl chains of C_{30} phases are more ordered than those of polymeric C_{18} phases.[20,21] A higher chain order increases the shape selectivity of the liquid chromatographic stationary phase exhibited for the above-mentioned compounds.

The correlation of solid-state NMR studies with LC data has provided a better understanding of the molecular shape selectivity of a series of polymeric long-chain reversed-phase materials, including C_{18}, C_{22}, and C_{30} phases.[20,22,23] Most of the explanations of chain structure and mobility were given in terms of ordered (trans conformations) and disordered (trans-gauche conformations) alkyl ligands. Still, a more qualitative and quantitative study on chain mobility and homogeneity of alkyl chain arrangement is required. It also remained unclear whether true self-assembled monolayers can be obtained on porous materials, whether there is a heterogeneity in chain arrangement (packing density), or whether even multiple layers are formed. The utilization of NMR chemical shifts, relaxation times, and spin diffusion parameters provides valuable tools[24] to address these questions and thus to get a better understanding of alkyl chain architecture.

Titania and zirconia provide an alternative to silica as chromatographic packing materials. These supports are superior to silica with respect to mechanical stability and chemical inertness within a pH range of 1−14.[25] Due to the different nature of surface OH groups, silanization is not as easy as for silica gels. The stability of a M−O−Si−R bond decreases in the order for M = Si, Zr, Ti, Al, and Nawrocki et al. concluded that silanized zirconia and titania would not be stable enough for LC applications.[25] Bonded zirconia and titania phases that were obtained though silanization with monochlorosilanes were found to be less stable than their silica-based counterparts. However, the use of trifunctional silanes resulted in reversed phases with enhanced stability.[26,27] So far, research has been focused only on C_{18}-modified titania[26,28,29] and zirconia.[26,27]

As an alternative approach for reversed-phase zirconia materials, ZrO_2 has been coated with polymers (e.g., polybutadiene).[30] These columns have proven to be useful for a variety of separations, particularly under demanding conditions such as high temperatures or high pH. The polybutadiene-coated zirconia offers shape selectivity properties that are similar to monomeric C_{18} phases.[30] As such they are not ideally suited for the separation of a series of isomeric compounds. Carotenoids, tocopherols, and vitamins A and K are better separated by stationary phases that exhibit enhanced shape recognition properties such as polymeric C_{18} phases or C_{30} phases.

Table 1. Properties of the Materials Used in This Study

support	particle size (μm)	mean pore size (Å)	pore vol (mL/g)	specific surf. area (m^2/g)	nom dens (g/cm^3)
silica A (LiChrospher)	3.0	300	0.74	77	2.2
silica B (ProntoSil)	3.0	260	0.90	109	2.2
titania (Sachtopore)	3.0	286	0.12	17	4.1
zirconia (ZirChrom Phase)	3.0	290	0.23	31	5.8

In this paper, we describe formation, microstructure, and application of C_{30} self-assembled monolayers on porous silica, titania, and zirconia. In an attempt to enhance phase stability against possible leaching, substrates were modified using surface polymerization silanization (i.e., the self-assembled monolayer approach).[31,32] According to this strategy, silanization is carried out on surfaces with a monolayer coverage of water. The resulting stationary phases are more homogeneously covered and offer high bonding densities.[22,23] We have chosen the C_{30} system because of its remarkable shape selectivity properties. The new bonded phases are characterized by ^{13}C and ^{1}H solid-state NMR spectroscopy. Atomic force microscopy (AFM), ellipsometry, and contact angle determination were utilized to study alkylsilane self-assembled monolayers on planar surfaces. Liqiud chromatography (LC) separations of polycyclic aromatic hydrocarbons (PAHs), carotenoids, and tocopherols were used to assess the performance of the C_{30} SAMs on different inorganic oxides as chromatographic stationary phases.

Experimental Section[1]

Certain commercial equipment, instruments, or materials are identified in this report to specify adequately the experimental procedure. Such identification does not imply recommendation or endorsement by the National Institute of Standards and Technology, nor does it imply that the materials or equipment identified are necessarily the best available for the purpose.

Synthesis. All inorganic oxides used for C_{30} SAM formation were of nominal 3-μm particle size and 300-Å pore size. The actual properties of these materials are listed in Table 1. LiChrospher (silica A) was obtained from Merck KGaA (Darmstadt, Germany) and ProtoSil (silica B) from Bischoff Chromtography (Leonberg, Germany). Titania (Sachtopore) was donated from Sachtleben AG (Duisburg, Germany) and zirconia (ZirChrom Phase) was received from ZirChrom Separations Inc. (Anoka, MN). *n*-Octadecyltrichlorosilane and *n*-triacontyltrichlorosilane were obtained from Gelest (Tullytown, PA) and United Chemical Technologies (Bristol, PA). The average chain length of the latter silane is C_{30}; however, according to the manufacturers, it contains a mixture of a mass fraction of 80% C_{30} and higher alkyl chains and 20% C_{22}−C_{28} chains.

The self-assembled monolayer synthesis was carried out as follows. The inorganic oxide materials were dried at 150 °C for 2 h. The resulting dry powders were equilibrated with humid air from 30 min up to 80 min (see Table 2) using a simplified apparatus similar to that described by Wirth and Fatunmbi.[31] Exposure time was adjusted to the surface area of the respective materials. The humidified inorganic oxides were then dispersed in 50 mL of xylene. Approximately 3.5 g of *n*-triacontyltrichlorosilane was dissolved in xylene (reflux), and the solution was filtered hot to remove solid impurities. The clear filtrate

(18) Strohschein, S.; Rentel, C.; Lacker, T.; Bayer, E.; Albert, K. *Anal. Chem.* **1999**, *71*, 1780−1785.
(19) Albert, K.; Lacker, T.; Raitza, M.; Pursch, M.; Egelhaaf, H. J.; Oelkrug, D. *Angew. Chem., Int. Ed.* **1998**, *37*, 777−780.
(20) Pursch, M.; Strohschein, S.; Handel, H.; Albert, K. *Anal. Chem.* **1996**, *68*, 386-393.
(21) Pursch, M.; Sander, L. C.; Albert, K. *Anal. Chem.* **1999**, *71*, 733A-741A.
(22) Pursch, M.; Sander, L. C.; Albert, K. *Anal. Chem.* **1996**, *68*, 4107−4113.
(23) Pursch, M.; Sander, L. C.; Egelhaaf, H. J.; Raitza, M.; Wise, S. A.; Oelkrug, D.; Albert, K. *J. Am. Chem. Soc.* **1999**, *121*, 3201−3213.
(24) Schmidt-Rohr, K.; Spiess, H. W. *Multidimensional Solid-State NMR and Polymers*; Academic Press: London, 1994;
(25) Nawrocki, J.; Rigney, M. P.; McCormick, A.; Carr, P. W. *J. Chromatogr., A* **1993**, *657*, 229−282.
(26) Truedinger, U.; Mueller, G.; Unger, K. K. *J. Chromatogr.* **1990**, *535*, 111−125.
(27) Yu, J.; El Rassi, Z. *J. Chromatogr.* **1993**, *631*, 91−106.
(28) Pesek, J. J.; Matyska, M. T.; Ramakrishnan, J. *Chromatographia* **1997**, *44*, 538−544.
(29) Ellwanger, A.; Matyska, M. T.; Albert, K.; Pesek, J. J. *Chromatographia* **1999**, *49*, 424−430.
(30) Li, J.; Carr, P. W. *Anal. Chem.* **1996**, *69*, 2857−2868.
(31) Wirth, M. J.; Fatunmbi, H. O. *Anal. Chem.* **1993**, *65*, 822−826.
(32) Sander, L. C.; Wise, S. A. *Anal. Chem.* **1995**, *67*, 3284−3292.

Table 2. Reaction Conditions and Properties of the Different C_{30} Self-Assembled Monolayers Used in This Study

support	equilbrn time with humid air (min)	% C of C_{30} SAM	surf. coverage (μmol/m^2)	$\alpha_{TBN/BaP}$	asymmetry TBN peak	efficiency (plates/m) TBN peak
silica (LiChrospher)	60	8.77	3.57	0.64	1.32	27 400
silica B (ProntoSil)	80	16.17	5.22	0.56	1.36	27 600
titania (Sachtopore)	30	3.58	6.10	0.44	1.69	28 400
zirconia (ZirChrom phase)	30	5.26	5.06	0.42	1.50	10 000

was then added to the slurry. The temperature was kept at 110−120 °C, and the mixture was shaken periodically. After 16−18 h, the mixture was refluxed for 30 min and then filtered hot. The bonded phases were washed with boiling xylene, then with acetone, ethanol, ethanol/water (1:1, v:v), water, ethanol, acetone, and pentane. Samples were shipped to Atlantic Microlab (Norcross, GA) for elemental analysis. Table 2 summarizes the properties of the four C_{30} SAMs.

C_{18} and C_{30} SAMs for AFM studies were prepared on silicon wafers. For this synthesis, a solution containing a volume fraction of 0.1% of either C_{18} or C_{30} trichlorosilane was prepared in anhydrous toluene. SAM formation was allowed to take place at ambient temperature and 4 h for C_{18} SAM and at 90 °C and 30 min for C_{30} SAM. After the exposure, the wafers were removed from the solution, washed with toluene (hot toluene for C_{30} SAM) several times, and dried with nitrogen. For comparison, a C_{30} SAM was prepared with a monochlorosilane using the same reaction conditions as for the C_{30} trichlorosilane.

Solid-State NMR. All ^{13}C spectra were taken at 25.2 MHz (2.35 T) on a noncommercial spectrometer equipped with a noncommercial probe whose 7-mm rotor/stator was manufactured by Doty Scientific, Inc. (Columbia, SC). ^{13}C Signals were acquired at ambient temperature under two conditions using magic angle spinning at 3.00 kHz. Either cross-polarization from the protons was used with a contact time of 1.5 ms or "Bloch decays" were acquired, following a single 90° pulse. The Bloch decay data were taken in the presence of Overhauser (OV) enhancement[33] as saturating pulses were applied to the protons, once every 5 ms, during the period between acquisitions. For comparison, we also acquired a few Bloch decay spectra in the absence of Overhauser enhancement. In each case, although the signal-to-noise ratio was inferior, the ratio of the two principal methylene resonances in the 30−34 ppm region was nearly the same, with or without the Overhauser enhancement. Hence, the Bloch decay spectra taken with Overhauser enhancement are regarded as being the most accurate indication of the relative amounts of the various carbons. Signal strength increased by a factor of 2.25 ± 0.10 in the presence of this pulsed proton saturation. Within the signal-to-noise, this factor also applied to the methyl (12−16 ppm) and the α-methylene (22−26 ppm) resonances. Radio frequency field strengths, expressed in terms of the nutation frequencies for the carbons and protons are 65 and 62 kHz, respectively.

Proton magic angle spinning (MAS) spectra of vacuum-dried SAM samples were acquired at 200 MHz (4.7 T) on a Bruker CXP200 spectrometer. The radio frequency amplitude gave a nutation frequency of 167 kHz (1.5-μs 90° pulse), and the spinning frequency was 2650 Hz unless otherwise indicated. Dead time was 2 μs. Average longitudinal relaxation times, T_1^H, were measured by identifying the delay time, τ_{null}, where initially inverted magnetization passed through zero on its way back to the Boltzmann equilibrium level [$T_1^H = \tau_{null}/\ln(2)$]. Since Bloch decay spectra consisted of both broad and narrow signals, spin diffusion spectra, which probe organizational heterogeneity over the sample, were also obtained. The motivation for the spin diffusion experiments was to probe the broader line shape for those protons that lay within a few tenths of nanometers of the mobile protons, and to see whether all, or just part, of the protons in the broad part of the line were such "neighbors" to these mobile protons. The spin diffusion experiment consisted of a pulse sequence where, initially, the narrow portion of the line is selected using a Carr−Purcell−Meiboom−Gill sequence[34] using a 2τ spacing between 180° pulses of 50 μs. At the third echo, the magnetization is alternately stored parallel or antiparallel to the static magnetic field direction. Then follows a variable period of spin diffusion, t_{sd}, terminated by a final 90° pulse that allows readout, accumulated by alternate addition and subtraction, of the state of the magnetization at the end of t_{sd}. Both the spatial movement of proton polarization via spin diffusion and T_1^H can contribute to the change in signal amplitude as a function of t_{sd}. In our analysis of the data in terms of spin diffusion, we made a correction for T_1^H contributions, assuming a uniform T_1^H throughout the sample. While the latter condition may not prevail, the correction based on the uniform T_1^H assumption is adequate for our purposes because our interpretation of the spin diffusion data is correspondingly semiquantitative.

^{13}C Chemical shifts were determined using the methine resonance in adamantane at 29.50 ppm (relative to tetramethylsilane, TMS) as an external standard.[35] Proton chemical shifts were determined by adding a tiny flake of poly(dimethylsiloxane) (shift, 0.1 ppm relative to TMS) to the center of a silica B sample.

Ellipsometry. The thin film thickness values were measured using a commercial spectroscopic ellipsometry (SE) system manufactured by the J. A. Woolam Co., Inc. (Lincoln, NE). The rotating analyzer/fixed polarizer SE system measures 44 wavelengths simultaneously from 1.6 to 3.0 eV. The SE measurements were performed in air, at an incidence angle of ∼75°, and with the polarizer at ±10° to average out first-order birefringence effects. The thin-film thickness was extracted by modeling the measured SE data using the commercial software package, WVASE32 (J. A. Woolam Co., Inc.). The two-layer model structure consisted of a thin film of thickness t and refractive index value $n = 1.5$ ($k = 0$), atop a silicon substrate. Model SE data were numerically generated from the Fresnel equations, literature values of the optical response of bulk silicon, and initial estimates for the film thickness and incidence angle. The values of the film thickness and incidence angle, and their 90% confidence limits, were obtained by optimizing those quantities to minimize the mean-squared error between the experimental and model-generated SE data. However, the resulting thickness values depend on the value of refractive index chosen for the film, because SE is only capable of measuring the product of the film thickness and refractive index, but not both independently. The refractive index values used in the model were chosen on the basis of published literature values of the measured optical properties of similar thin films. By using the same refractive index value for all of the films, the relative thickness of different films can be compared using SE. However, these values do not necessarily reflect the true values of the experimental accuracy of this technique.

AFM. Tapping mode atomic force microscopy was performed with a Dimension 3100 Nanoscope III (Digital Instruments, Santa Barbara, CA) scanning probe microscope. Topographic (height) images were recorded at ambient conditions. Commercial silicon cantilever probes, each with a nominal tip radius of 5−10 nm and a spring constant in the range of 20−100 N/m, were oscillated at their fundamental resonance frequencies, which ranged between 250 kHz. The setpoint voltage values were 80−90% of the free amplitude. The images were flattened and no other filtering was done before analyzing their roughnesses. The mean roughness, R_a, is calculated as

$$R_a = (L_x L_y)^{-1} \int_0^{L_x} \int_0^{L_y} f(x,y)\, dx\, dy \qquad (1)$$

where L_x, L_y are the dimensions of the surface and $f(x,y)$ is the surface relative to the center plane.

Contact Angle Measurement. Contact angles of C_{18} and C_{30} SAMs on silicon wafers were measured using a Rame-Hart goniometer. Both advancing and receding angles of water and methylene iodide were recorded ∼30 s after placing the drop on the sample surface. A minimum of six readings was recorded for each liquid on each sample.

(33) Overhauser, A. W. *Phys. Rev.* **1953**, *92*, 411.
(34) Meiboom, S.; Gill, D. *Rev. Sci. Instrum.* **1958**, *29*, 688.
(35) Earl, W. L.; Vanderhart, D. L. *J. Magn. Reson.* **1982**, *48*, 35−54.

The polar force components of the film were estimated using the geometric means approach of Owens and Wendt.[36] In this approach, the polar and nonpolar or dispersion force components of a material are calculated based on contact angle data and the polar and nonpolar components of surface tension for the two liquids. Surface tension values of 72.8 and 50.8 mJ/m^2 for water and methylene iodide,[37] respectively, and their respective polar component values of 50.7 and 1.8 mJ/m^2 were used for the calculation.

Column Packing. The bonded phases were slurried in 30 mL of 2-propanol and packed with 2-propanol at 75 MPa in stainless steel columns (25 cm × 4.6 mm i.d.; for ZrO_2-C_{30} 15 cm × 2 mm i.d.). It should be noted that the column packing procedure was not optimized for the TiO_2 and for the ZrO_2 C_{30} materials. Because the density of these materials is significantly greater than silica substrates, it is likely that settling occurred before the packing was complete and the resulting column efficiencies are lower. The densities of titania and zirconia are 4.1 and 5.8 g/cm^3, respectively, compared with 2.2 g/cm^3 for silica gel.

Liquid Chromatography. All separations were carried out with a Varian model 5000 liquid chromatograph (Varian Inc., Walnut Creek, CA). Standard Reference Material (SRM) 869a Column Selectivity Test Mixture for Liquid Chromatography and SRM 1647c Priority Pollutant Polycyclic Aromatic Hydrocarbons were obtained from the Standard Reference Materials Program (NIST, Gaithersburg, MD). α-, *β*-, *γ*-, and *δ*-tocopherol were received from Merck KGaA (Darmstadt, Germany). *β*-Carotene and zeaxanthin were received from Sigma (St. Louis, MO) and Hoffman-La Roche (Basel, Switzerland), respectively. The carotenoid standards were isomerized with a solution of iodine in *n*-hexane according to the procedure described by Zechmeister.[38]

Results and Discussion

The reaction conditions for preparation of C_{30} SAMs and their properties are summarized in Table 2. Differences in absolute carbon content among the samples are the result of different surface areas of the substrates. All SAM materials possess high surface coverages varying from 3.57 (LiChrospher C_{30}) to 6.1 *μ*mol/m^2 (TiO_2 C_{30}). Although titania and zirconia possess different quantities of surface OH groups than silica, the surface polymerization reaction utilized does not strongly depend on the native OH groups for silanization. Adsorbed water molecules promote silane polymerization at the surface, which is thought to result in a physically immobilized phase with occasional covalent bond linkages to the surface. A series of inorganic oxides was investigated by Jaroniec et al., who found less water adsorbed on LiChrospher compared to native titania and zirconia.[39] The silica A (LiChrospher) shows the lowest ligand density (3.57 *μ*mol/m^2), which is likely to have resulted from a lower adsorption of water (at the time of SAM formation) than with the other substrates. An incomplete layer of water may reduce the number of sites for hydrolysis and for cross-linking of the C_{30} silane ligands.

^{13}C Solid-State NMR Spectroscopy. ^{13}C Solid-state NMR spectra (CP/MAS and Overhauser-enhanced MAS) of the four C_{30} self-assembled monolayers are shown in Figure 1. The main resonances at 33.4 and 30.6 ppm originate from the interior $(CH_2)_n$ groups and have been attributed to conformationally more ordered ("trans") and less-ordered (dynamically disordered "trans-gauche") regions, respectively.[20,23] Regarding the generation of ^{13}C signals, employment of the technique of cross-polarization in CP/MAS NMR spectra tends to produce a good signal-to-noise ratio. At the same time, mobile species are

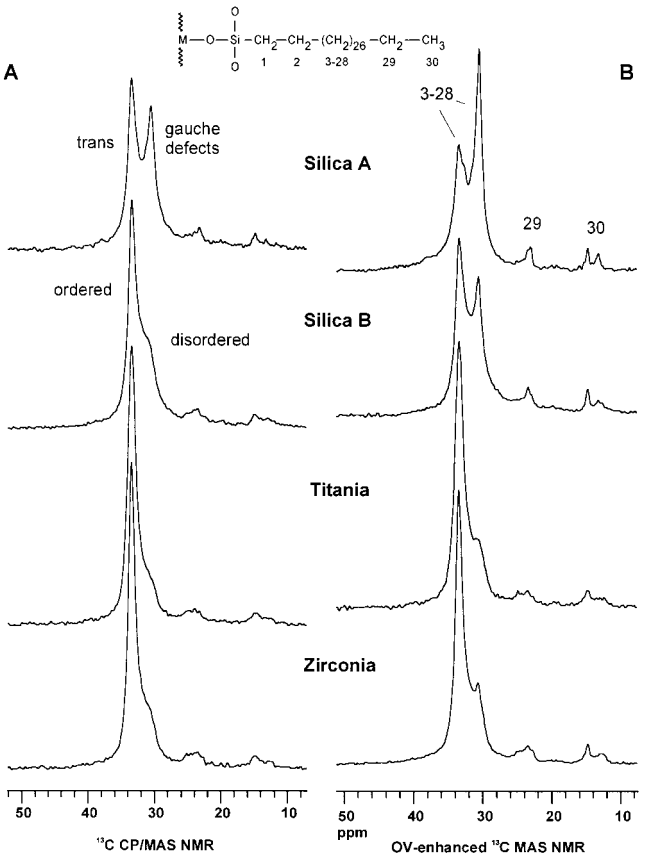

Figure 1. (A) 25 MHz, ambient temperature ^{13}C CP/MAS NMR and (B) Overhauser-enhanced MAS NMR spectra of dried C_{30} self-assembled monolayers prepared on inorganic oxides.

usually underrepresented in such NMR spectra (Figure 1A), although the extent of line shape distortion depends on cross polarization efficiency, the contact time, and the local rotating frame proton relaxation time, $T_{1\rho}{}^{H}$; we used 1.5-ms contact time. For the materials we studied, more representative, low-distortion line shapes are associated with Bloch decay spectra in the presence of Overhauser enhancements (Figure 1B). For the same sample, the latter spectra consistently show an increase in the trans-gauche peak relative to the trans peak compared to CP spectra. A trend in chain order is found for the C_{30} SAMs. The signal for trans conformations is relatively more intense for the titania and zirconia bonded phases than for the silica-bonded C_{30} materials. This indicates that the trans conformation is more strongly favored for the interior methylenes of the C_{30} SAMs on the TiO_2 and ZrO_2 phases. The ^{13}C MAS NMR spectrum of the silica A C_{30} SAM shows the highest trans-gauche fraction.

It is of interest to discuss the properties of the trans signal in more detail since one might be tempted to assign "crystal-like" organization to the carbons giving rise to these signals (as is the case in alkanes, e.g., $C_{19}H_{40}$, $C_{23}H_{48}$, or $C_{32}H_{66}$). The chemical shift (CS) at 2.35 T for the trans peaks of the C_{30} SAMs (33.4 ppm) is nearly identical to that of the interior methylene carbons (IMCs) in the C_{19} alkane. At ambient temperature, C_{19} exists in the rotator phase with a hexagonal unit cell where the chains undergo fast diffusional rotation around their long axes. The CS of the IMCs in the normal orthorhombic (e.g., C_{23} alkane) or monoclinic (e.g., C_{32} alkane) unit cell is ∼33.1 ppm, i.e., 0.3 ppm lower. The two-chain unit cells in these latter crystal structures offer environments around the IMCs that are essentially identical to one another; moreover, there are no large-amplitude fast motions at ambient temperature. Relative to the remaining alkane crystal phase, namely, the

(36) Owens, D. K.; Wendt, R. C. *J. Appl. Polym. Sci.* **1969**, *13*, 1741.
(37) Wu, S. *Polymer Interface and Adhesion*; Marcel Dekker: New York, 1982; p 151.
(38) Zechmeister, L.; Polgar, A. *J. Am. Chem. Soc.* **1943**, *65*, 1522−1528.
(39) Jaroniec, C. P.; Jaroniec, M.; Kruk, M. *J. Chromatogr., A* **1998**, *797*, 93−102.

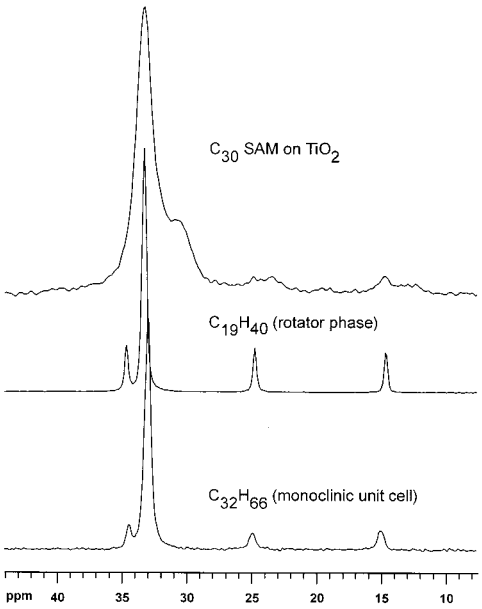

Figure 2. ^{13}C Spectra of the materials indicated. The SAM spectrum is Overhauser-enhanced. The remaining spectra are CP/MAS. Note the better overlap of the SAM resonances with the C_{19} resonances (rotator phase) than with the C_{32} (rigid crystal phase) resonances.

triclinic phase (e.g., C_{20}) which has just one molecule per unit cell, the 33.4 ppm SAM CS is very different,[40,41] i.e., 1.0 ppm lower. In Figure 2the OV-enhanced spectrum of the C_{30} titania SAM is compared with the C_{19} and C_{32} alkane CP/MAS spectra. Note that the IMC chemical shift correspondence between the C_{19} carbons and the titania SAM carbons carries over to the positions of the terminal methyl carbon and the α-methylene carbon, at least to the downfield maximums of these SAM resonances. Note also that the line width of the trans peak for the titania SAM is ~3 times wider than for the corresponding IMC resonances in C_{19} and C_{32}. The greater line width of the SAM resonances suggests more disorder (more chemical shift dispersion) and/or more mobility (causing line broadening) than any of the crystal phases, including the rotator phase.

Another qualitative measure of molecular mobility is the ^{13}C longitudinal relaxation time, T_1^C. T_1^C data at 25 MHz (Table 3), determined by the inversion recovery sequence for the C_{30} SAM on silica B, reveal that the alkyl chains, despite their implied order, are still rather mobile. T_1^C values are very similar for both of the IMC signals, namely, 250−300 ms for the trans-gauche peak (30.5 ppm) and 350−400 ms for the trans peak (33.3 ppm). In Table 3, these T_1^C values are compared to those of the IMCs in C_{19}, C_{23}, and C_{32}. The significantly shorter T_1^C's for the silica B sample, compared to the C_{23} and the C_{32} alkanes, indicate that the chains in the silica B are much more mobile than these alkane chains. A crude upper limit on the correlation time implied by a 400-ms T_1^C can be calculated.[42] Assuming that the ^{13}C relaxation is dipolar and the reorientational motion of the $^{13}C-^{1}H$ vectors is diffusive and isotropic, the reorientational correlation time, τ_c, is less than 2.3×10^{-7} s. We did not measure the T_1^C's of all of the samples; however, we have a general sense (from measurements of Overhauser signal amplitudes at two delay times) that for the zirconia sample, which has a more ordered SAM than for silica B, $T_1^C < 800$ ms for the trans peak ($\tau_c < 4.6 \times 10^{-7}$). It is important to recognize the dynamic character of these "trans" methylenes. Ostensibly they have a strong bias, in a time-average sense, toward adopting the trans conformation; however, they are also undergoing large-amplitude reorientational fluctuations on time scales of a few tenths of microseconds or less. At the same time, we cannot insist that these rather fast motions necessarily involve conformational interconversions as opposed, for example, to rotation about the chain axes. Indeed, the chemical shift similarities to C_{19} might argue for a stronger consideration of chain rotation. Nevertheless, we do not dismiss the possibility of some conformational interconversion, so long as the time-average conformation remains near the 'trans' conformation.

The final ^{13}C observations we discuss relate particularly to the shape of the terminal methyl resonances and less directly to the question of heterogeneity in the density of chain packing. This terminal methyl carbon we have called no. 30 for convenience, even though there is a distribution of chain lengths in this C_{30} SAM (see Experimental Section). Since the NMR spectra are correlated with LC performance, it is of interest to understand as much as possible about the nature of the SAM structure, especially its surface. The methyl resonance is discussed in detail because this resonance may contain significant information about surface organization. We hope that this discussion together with future work might establish the interpretation of the methyl line shape as an important characterization tool for these alkane-type SAMs.

In Figure 1, it is clear that the methyl resonances in all of the SAM preparations are quite broad, spanning the range from about 12 to 16 ppm. This is true of both the Overhauser Bloc -decay spectra and the CP/MAS spectra. Moreover, in Figure 1, there is often a distinct double maximum associated with this resonance; this characteristic is generally seen more clearly in the Overhauser spectra. Figure 3 shows the two silica B spectra of Figure 1 with greater vertical expansion along with a difference spectrum. The difference spectrum emphasizes those carbons which had the most difficulty cross-polarizing because (a) all resonances are measured to have very similar Overhauser enhancements and (b) the relative vertical scaling was chosen to equalize the signal contributions from the "trans" portion of the line shape, i.e., the more rigid molecules. Difficulty in cross-polarizing can arise mainly for two reasons for alkane-type molecules. First, the density of motions in the mid-kilohertz regime may be high and this would typically shorten $T_{1\rho}^H$ to values of 1 ms or less. In other words, the proton polarization would be held for a time too short to allow for good polarization transfer to the carbons. Such a condition is usually accompanied by substantial spectral broadening of the carbon resonances because such motions would also interfere with decoupling.[43] Second, this cross-polarization depends on the existence of carbon−proton dipolar couplings, and, less obviously, on proton−proton dipolar couplings.[44] Therefore, fast motions, with sufficiently large amplitude, could reduce the residual, motionally averaged static dipolar couplings, both inter- and intramolecular, to sufficiently small values that polarization transfer would become very inefficient. Because the difference spectrum of Figure 3 consists mainly of sharper spectral features, the second reason, namely, fast motions and weak dipolar couplings, constitutes the main reason for the resonances in the difference spectrum.

In Figure 3, the methyl resonance profiles all display double maximums positioned at CSs of 14.7 and ~13 ppm. The 14.7

(40) Vanderhart, D. L. *J. Magn. Reson.* **1981**, *44*, 117−125.
(41) Vanderhart, D. L. *J. Chem. Phys.* **1986**, *84*, 1196−1205.
(42) Abragam, A. *The principles of nuclear magnetism*; Oxford University Press: London, 1961; pp 294−297.
(43) Vanderhart, D. L.; Earl, W. L.; Garroway, A. N. *J. Magn. Reson.* **1981**, *44*, 361−401.
(44) Steijskal, E. O.; Schaefer, J.; Waugh, J. S. *J. Magn. Reson.* **1977**, *28*, 105.

Table 3. ^{13}C T_1 Relaxation Parameter for Immobilized and Crystalline Alkyl Chains

CH_2 resonance	ProntoSil C_{30} (33.3 ppm)	ProntoSil C_{30} (30.5 ppm)	$C_{19}H_{40}$	$C_{23}H_{48}$	$C_{32}H_{66}$
properties	amorphous, more ordered	amorphous, more disordered	hexagonal, rotator phase	orthorhombic	monoclinic
^{13}C T_1 value (s)	0.35−0.4	0.25−0.3	1.71	14.9	184

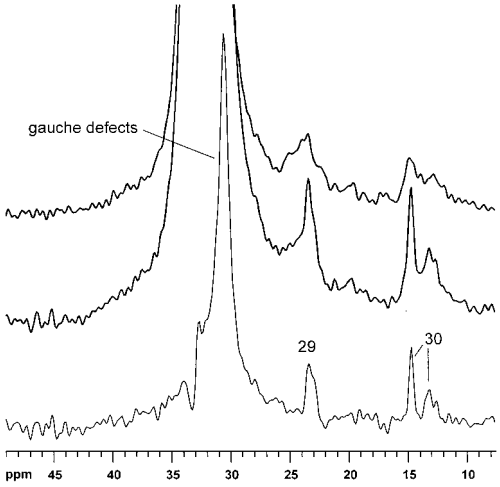

Figure 3. Vertically amplified ^{13}C spectra of the C_{30} SAM on silica B. Upper trace, CP/MAS; middle trace, Overhauser-enhanced; lower trace, difference. Vertical scaling is chosen to minimize "all-trans" methylene contributions near 33.4 ppm. The difference spectrum represents those carbons that cross-polarize with the most difficulty, especially for reasons of high mobility. Carbons "29" and "30",, respectively, refer to the terminal methylene and methyl carbons at the free end of the tethered chains which are, for simplicity of nomenclature, assumed to be 30 carbons long.

ppm shift is the same as the methyl shift for C_{19}; it is also ~0.3 ppm less than the methyl shifts of crystalline C_{23} and C_{32}. A similar shift upfield was noted for chain-end methyl groups in polyethylene in going from a crystalline to a noncrystalline environment.[45] Thus, the 14.7 ppm shift is not unusual and suggests an environment less ordered than a rigid crystal.

The 13 ppm resonance is a different matter. To our knowledge, no long-chain-alkane methyl carbon resonates at such a high-field position in either a crystalline or a noncrystalline environment. However, dual methyl resonance maximums, similar to those shown, have been observed before in surface layers involving alkane-type molecules. Gao et al. noted dual maximums in octadecylphosphonic acid monolayers on both zirconated silica and alumina.[46] Interestingly, they saw *only* the 13 ppm peak in monolayers of this acid on nonporous titania and zirconia. They concluded that the methyls resonating at 13 ppm could be assigned to organic/air interfaces while the methyls in the 14−15 ppm range were methyls completely surrounded by other organic molecules; i.e., these latter methyls were, in their opinion, nonsurface methyls that originated from multilayer regions. Further support for the assignment of the 13 ppm peak to methyls at organic/air interfaces comes from another study[17] where ^{13}C spectra of a C_{30} bonded phase, similar to the materials of the present study, were taken both in the dry state and with different organic solvents present. In the dry state, two methyl peaks were observed, while the presence of each solvent, in turn, led to a shift of all methyl resonances to the position of the lower-field peak near 14.7 ppm. Both of the foregoing studies support the assignment of the high-field methyl peak to methyls at the organic/air interface. In our interpretation of the resonance covering the 12−16 ppm region, we will asume that all of the features arise from methyl carbons and that the 13 ppm portion of this resonance represents methyl carbons that are only partially surrounded by organic molecules because they lie near an air interface in the dry state.

Before we proceed with our interpretation of the methyl resonance, we digress to explore the possibility that the "C1" carbon, which is attached to the Si atom at the tethered end of the chain, might also contribute intensity to this region since its resonance is also expected to lie in the vicinity of the methyl carbon. First, in the work just cited,[17] the loss of the 13 ppm resonance in the presence of solvents, including polar methanol, strongly suggests that the 13 ppm peak belongs to the methyl carbon and not to C1. As to the possibility that C1 contributes strongly to the 14.7 ppm region, we depend on less direct evidence, namely, that the fractional contribution of the 12−16 ppm region to the total integral in each Bloch decay spectrum is very close to 0.033, as expected for a resonance representing a single carbon. (The Overhauser enhancement factor for this methyl resonance is, within experimental error, the same as for the large, central methylene lines.) Also, the 14.7 ppm shift is very commonly found for chain-end methyl resonances in bulk phases. The corollary to the above comments is that the real C1 resonance must be very broad, probably owing to the mobility restrictions from being so close to the point of tethering.

With this perspective, we return to Figure 3 and note first that a certain fraction of the methyls in both peaks have sufficiently limited mobility to cross-polarize. Second, we note in the Overhauser spectrum, and especially in the difference spectrum, that the most mobile methyls also contribute to both peaks, albeit the resonance width for both peaks is, on average, narrower for the more mobile than for the less mobile methyl carbons. Thus, while we might naively expect a correlation between the extent of mobility and position at the surface, this correlation is only weak, if it exists at all. Also, if we apply the interpretation that Gao et al. gave to the 13 ppm peak, this would imply that, in all of these preparations, a half, or more, of the material exists in a multilayer structure. Given that the coverage implied by the surface area measurements combined with the organic assays always implied less than a full monolayer coverage in these materials**,** extensive multilayer structures would further imply that significant portions of the surface were either bare or had very low density of coverage. The AFM results, discussed below, for flat substrates of silicon prepared in the same way these porous samples were, identify some multilayered regions but they are not dominant. Hence, we look for alternate reasons, compatible with a dominant monolayer structure, for explaining why the 14.7 ppm line is so intense in these materials.

We strongly suspect that in these materials, which have a distribution of chain lengths around the C_{30} length, there is little segregation of chains on the basis of length; rather, the different lengths are pretty well mixed, probably because (a) reaction during SAM formation likely takes place according to the availability of reactants and (b) the presence of solvents during SAM formation reduces the thermodynamic driving forces for

(45) Perez, E.; Vanderhart, D. L. *J. Polym. Sci. B* **1987**, *25*, 1637−1653.
(46) Gao, W.; Dickinson, L.; Grozinger, C.; Morin, F. G.; Reven, L. *Langmuir* **1996**, *12*, 6429−6435.

segregation. In addition, tethering does not allow for any subsequent diffusion-driven lowering of the free energy by sorting the chain lengths. Thus, we imagine that the shorter chains in a densely packed monolayer might have their methyl resonance at 14.7 ppm because these methyls are surrounded by organic moieties that primarily consist of residues, near the free ends, of longer neighboring chains. (Support for this interpretation also comes from CPMAS spectra of C_{18} SAMs on silica[22] where, presumably because of uniform C_{18} chain lengths, there would be significantly fewer methyls buried below the surface. In this case, no distinct peak at 14.7 ppm is observed; there is only a broad downfield shoulder for the 13 ppm resonance.) At the same time, owing to the dense packing, these methyl carbons on the shorter chains would probably have sufficient dipolar interactions for cross-polarizing. The methyl carbons on the longer chains in such an area of dense packing would probably exhibit an average mobility and an upfield shift, both of which increase with chain length, the shift being the result of a greater proximity to the air interface. Conceivably, the intermediate chain lengths might have sufficiently strong dipolar interactions to contribute to the CP/MAS intensity near 13 ppm. But then, how does one get highly mobile carbons to contribute to the 14.7 ppm line as is demonstrated in the difference spectrum of Figure 3? And what is the origin of the very mobile methyl carbons that resonate at 13 ppm?

We propose two possibilities for mobile methyls at 14.7 ppm. First, if there are some multilayer structures, it is likely that a bilayer structure would form because of the amphiphilic nature of the C_{30} SAM molecules. Thus, all methyls in such a bilayer would share approximately the same elevation within the layer. Moreover, the effective molecular weight of any molecules that are not tethered to the surface could be rather small. Such molecules might possess significant translational mobility, which, in turn, could reduce the important intermolecular dipolar couplings to protons. Second, assuming two conditions, namely, that (a) mostly "monolayer" regions exist and (b) variations in chain density from one surface region to another exist, one could imagine having a density sufficiently low that chains would be in a dynamic state of collapse such that methyls would be found, on average, surrounded by organic moieties. In this case, one would expect a mobility for these methyls that is much greater than for the shorter-chain methyls in a more densely packed surface.

What, then, might be the morphological origin for highly mobile methyls resonating at 13 ppm? By inspection of Figures 1 and 3, it appears that the population of these methyls is highest in silica A and in silica B, the samples with the lowest packing densities and the lowest fractions of "trans" methylene carbons. One suggestion is that the mobile, 13 ppm methyls are identified with chains in regions of such low packing density that one would have high mobility but would not have a very dense environment of organic moieties. For these chains, more carbons than simply the methyl carbons would be expected to have shifts characteristic of an air interface. Another suggestion is that these methyls are associated with the longest chains in medium- to high-density layers, but this is less consistent with silicas A and B having the highest populations of these methyls.

If we look for other clues from non-methyl resonances for the interpretation of the methyl resonances, we note that, in the difference spectrum of Figure 3, the width of the "trans-gauche" peak is quite narrow, suggesting that high mobility is not confined completely to chain ends. At the same time, we do not see any evidence for upfield shifts that might indicate interior methylene carbons in very low-density environments that might have some shift contribution from air interfaces. Also, for the α-methylene resonance at 22−26 ppm, the overall width of this resonance, seen most clearly in the CP/MAS spectrum, suggests a rather wide dispersion of environments. The low-field and rather weak shoulder at ∼24.8 ppm coincides in chemical shift with the 24.8, 25.1, and 24.9 ppm shifts of the α-methylene carbons in C_{19}, C_{23}, and C_{32}, respectively. However, the resonance maximum at 23.4 ppm is more typical of disordered environments. The high-field shoulder in the CP/MAS spectrum may reflect some air−interface contribution. In principle, C2 resonance contributions are also expected in this region, but relative integrals in the Bloch decay spectra again suggest that mainly one carbon is contributing.

To summarize the inferences based on the ^{13}C CSs, T_1^C, and the methyl carbon line shapes, the picture that emerges is as follows: First, there is a reasonable correspondence between the CSs of the C_{19} molecules and a subset of the C_{30}-SAM resonances. Second, T_1^C measurements indicate large-amplitude motions (probably anisotropic) at ambient temperature on a time scale of microseconds or shorter for all carbons. So the dynamic processes are both fast and pervasive. Third, on the basis of the methyl carbon line shapes, there could be some multilayer or bilayer character in these preparations. Also, the appearance of the surface, even for the more densely covered surfaces, is probably quite textured on a scale of, say, 0.3−0.7 nm, owing to the distribution of chain lengths (see AFM section). Finally, there is a relatively strong suggestion that significant variations in packing density are present in order to explain the variations in both mobility and CS of these methyl carbons. But we have no indication of the distance scale over which such variations are to be found. We note in passing that when Gao et al. observed only a 13 ppm methyl resonance for octadecylphosphonic acid monolayers on nonporous titania and zirconia,[46] we presume that those monolayers differed from ours in two important ways: (a) they had no variations in chain length and (b) the density of the coverage in their monolayer was quite high and reasonably uniform, possibly because all their surfaces were external and easily accessible to the reactants.

Characterization of C_{18} and C_{30} SAMs by Atomic Force Microscopy, Contact Angle, and Ellipsometry Measurements. Some important information on heterogeneity of films on planar surfaces can be obtained by AFM. Bierbaum et al. studied the growth behavior as well as film properties of C_3, C_{18}, and C_{30} SAMs using near-edge X-ray absorption fine structure (NEXAFS) spectroscopy, AFM, and ellipsometry.[7,8] Their results support the "island model", which concludes that incomplete monolayers result from the presence of partially ordered islands and not from homogeneous, low-density coverage.[47] Our preparation of the C_{30} SAM differed in that we allowed SAM formation to occur at elevated temperatures (90 °C) in order to have reaction conditions similar to those for the porous materials. Figure 4 illustrates AFM images (1-μm^2 area) of C_{18} and C_{30} SAMs. For comparison, the C_{18} monolayer is very smooth; its surface roughness is smaller than 0.09 nm. A much higher surface roughness (0.77 nm) was determined for the C_{30} SAM, which is on the order of about five C−C bonds. This might be due to the chain length distribution in the C_{30} silane, varying from C_{22} to C_{36} (approximately) which is very likely to increase surface texture. AFM images of larger areas (10 μm) indicate the presence of adsorbed particles or clusters (average height 7−10 nm) on the C_{30} SAM. Keeping in mind the length of an extended C_{30} silane ligand (4.2 nm), it is

(47) Cohen, S. R.; Naaman, R.; Sagiv, J. *J. Phys. Chem.* **1986**, *90*, 3054−3056.

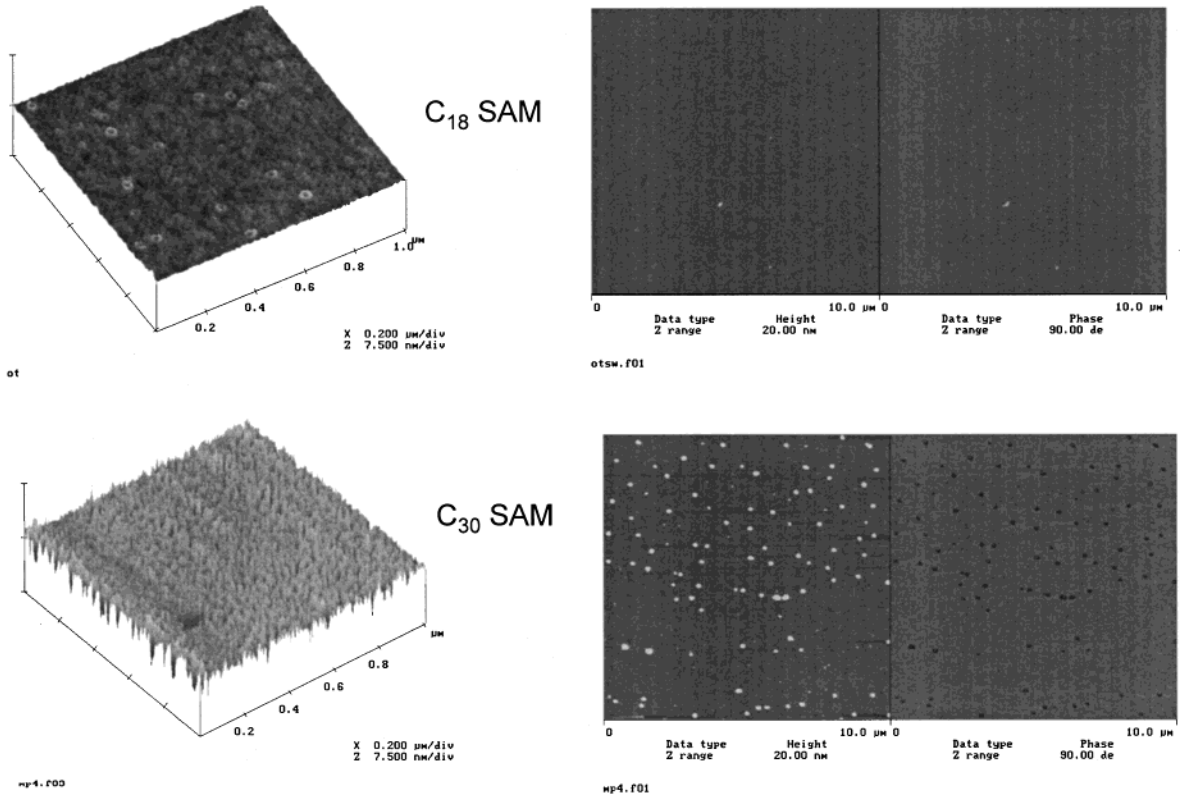

Figure 4. AFM images of C_{18} and C_{30} self-assembled monolayers.

Table 4. Film Thicknesses Determined by Ellipsometry, Contact Angle of Water, Surface Free Energy Parameters, and Polarity of C_{18} and C_{30} SAMs[a]

		contact angle of water (deg)					
	thickness (nm)	Θ_{adv}	Θ_{rec}	γ^d (mJ/m^2)	γ^p (mJ/m^2)	γ (mJ/m^2)	χ^P
C_{18} SAM	2.82 ± 0.04	109 ± 1	97 ± 1	26.23	0.01	26.24	0.0004
C_{30} SAM[b]	4.06 ± 0.02	103 ± 1	87 ± 1	27.87	0.25	28.12	0.009
C_{30} SAM[c]	2.11 ± 0.04	70 ± 2	52 ± 4	27.92	11.46	39.38	0.291

[a] θ_{adv}, advancing contact angle of water; θ_{rec}, receding contact angle of water; γ^d, nonpolar component; γ^p, polar component; γ, total surface free energy; $\chi^p = \gamma^p/\gamma$, polarity. [b] Prepared using a trichlorosilane [c] Prepared using a monochlorosilane.

reasonable that multilayers or clusters are formed. Although these clusters lead to some heterogeneity, they only amount to 2% of the surface area of the C_{30} monolayer. In addition, the average diameter of these clusters is 150 nm, which is considerably larger than the pore size of the porous materials (26−30 nm). From these two observations we would expect that cluster formation on porous silica, titania, and zirconia does not occur to a large extent.

Ellipsometry is widely used to determine thicknesses of thin films.[48−51]

Table 4 contains ellipsometry data of a C_{18} SAM and two C_{30} SAMs that were prepared with a monochloro- and a trichlorosilane. The thickness of a C_{18} SAM amounts to 2.82 nm and corresponds to the theoretical value with fully extended C_{18} chains. The trichlorosilane C_{30} SAM has a thickness of 4.05 nm, slightly lower than the expected value of 4.25 nm.[8] Ellipsometry provides an average thickness value, and if we take into account that some multilayers are present on the surface, the residual "monolayer" is somewhat incomplete. This is also indicated by the surface coverage values and NMR data for the porous materials, where the surface accessibility for long-chain silanes might be more difficult. Interestingly, a very thin film (2.1 nm) is formed by reaction with the C_{30} monochlorosilane. Compared to a trichlorosilane, the reactivity of the monochlorosilane is lower and the reaction time was probably not long enough to allow complete monolayer formation. In addition, the CH_3 groups attached to the silicon atom prevent the C_{30} chains from close packing. This induces a higher chain disorder and a smaller film thickness would be expected.

The water advancing contact angle of the C_{18} film was $109 \pm 1°$ (Table 4), which is slightly lower than a value of $112 \pm 2°$ reported previously for this material before or after annealing.[51] This result, together with the essentially zero value of the surface free-energy polar component (γ^p), indicates that the formation of the C_{18} layer was mostly complete and that the film was highly hydrophobic. This interpretation is consistent with AFM data showing a very uniform, smooth surface (roughness <0.09 nm). The advancing contact angle of the C_{30} film prepared from trichlorosilane was slightly lower than that of the C_{18} SAM. However, the receding angle of this film was substantially lower and the contact angle hysteresis ($\theta_{adv} - \theta_{rec}$) was greater compared to the C_{18} SAM. Because receding contact angle is sensitive to high-energy material (e.g., polar species)

(48) Semal, S.; Voue, M.; de Ruijter, M. J.; Dehuit, J.; Coninck, J. *J. Phys. Chem. B.* **1999**, *103*, 4854−4861.
(49) Rye, R. R.; Nelson, G. C.; Dugger, M. T. *Langmuir* **1997**, *13*, 2965−2972.
(50) Engquist, I.; Lestelius, M.; Liedberg, B. *Langmuir* **1997**, *13*, 4003−4012.
(51) Calistri-Yeh, M.; Kramer, E. J.; Sharma, R.; Zhao, W.; Rafailovich, M. H.; Sokolov, J.; Brock, J. D. *Langmuir* **1996**, *12*, 2755.

and the hysteresis is caused by both surface roughness and chemical heterogeneity in a film, the results suggest that surface coverage of the C_{30} SAM was not uniform and/or incomplete. This may be due to chain length distribution in the film or clustering, as postulated earlier in the AFM section. Further, since the γ^p value of this sample was very low, the effect of chemical heterogeneity on the hysteresis and the fraction of uncovered substrate surface in this film should be small. This is consistent with the small fraction of clustering (2%), as revealed by AFM images. The greater and more homogeneous coverage of the C_{18} than the C_{30} SAM may be due to the greater reactivity of the former toward SiO_2 than the latter, as reported by Bierbaum et al.[8]

On the other hand, the surface of the C_{30} sample prepared from monochlorosilane had a relatively low water contact angle, high polarity, and high contact angle hysteresis, indicating the highly inhomogeneous nature of this sample surface. Comparing the total surface free energy (γ) value of this film with that of the C_{30} SAM prepared from trichlorosilane or C_{18} film reveals that the good wettability of this sample was due solely to an increase in the polar component. This result suggests that a substantial surface area of this sample was not covered and that the uncovered hydroxylated SiO_2 layer on the surface of the silicon wafer contributed to the low water contact angle and high polarity of this sample.

Solid-State Proton NMR Spectroscopy. At this point, we discuss, in a rather qualitative way, several proton NMR results that are pertinent to our understanding of two separate issues, namely, the general mobility of chains and possible heterogeneity in the density of coverage. The latter issue is relevant to these preparations since, at the time of SAM preparation, the chemical reaction takes place mainly in the labyrinthine interior of the particles. It is not obvious that the supply of reactants or the chemical environment is the same for reactions taking place near the outer surface of these particles as opposed to deep in the interior of the particles.

In the following discussion, we note considerable heterogeneity of mobility. We suggest that such heterogeneity is to be expected for reasons of (a) tethering of the C_{30} molecules at one end only, (b) a distribution in alkane lengths in the reactant mixture, and (c) possible variations in the overall density of the SAM layer from region to region. Obviously we cannot separate all of the above contributions and whatever we say about mobility must be scrutinized for contributions from any or all of the above sources of mobility. One of the motivations in performing the spin diffusion measurements was to determine that item c is not negligible.

Besides T_1^C, a further measure of the mobility of the interior methylenes is the proton line width, which, for rigid alkanes (or polyethylene crystalline regions) amounts to 60 kHz and for C_{23} to 53 kHz. In Figure 5, Bloch decay spectra at a MAS frequency, ν_r, of 2650 Hz are overlaid for three samples, namely, the titaniaSAM, C_{19}, and pressure-crystallized polyethylene (PC-PE). Crystallinity exceeds 90% for the latter material. These spectra are normalized to approximately equal peak amplitudes for the broad components. The C_{19} represents the rotator phase and the PC-PE represents a rigid, long-chain-alkane lattice. The titania spectrum consists of a broader and a narrower component, the latter split into spinning sidebands, separated by the spinning frequency. It is evident that the broader portion of the line shape of the titania protons is much narrower than that of PC-PE. Simply by inspection of the line widths of PC-PE and the titania SAM, one immediately surmises that significant, large-amplitude motional averaging is taking place on a time scale of a few

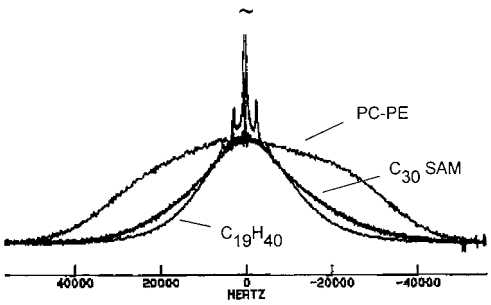

Figure 5. Overlay of three 200-MHz Bloch decay line shapes to illustrate fast partial averaging of the dipolar interactions in C_{30} SAM on titania. The wide line with no central peaks is pressure-crystallized polyethylene; this is the spectrum of a rigid, long-chain alkane lattice. The line narrowest at the base with a small central glitch from an impurity is that of C_{19}, representing a rotator phase. The remaining line with the strong central feature is that of the C_{30} SAM on titania.

microseconds or less and that most, if not all, of the protons participate. The foregoing is consistent with deductions from T_1^C data. It is hard to define precisely what the line width is for the broad component in the titania spectrum since one must choose a baseline beneath the spinning centerband and the sidebands. Nevertheless, the broad component line width is about 23−26 kHz, compared to 60 kHz for PC-PE, 53 kHz for C_{23} (not shown), and 23 kHz for the C_{19} rotator phase. Another important qualitative point about Figure 5 is that the broad portion of the titania SAM spectrum has somewhat wider wings than that of the C_{19} rotator protons although the central portion of the titania SAM spectrum, which lies beneath the narrow centerband and spinning sidebands, seems narrower than for C_{19}. Therefore, while the average line widths of the titania SAM spectrum and the C_{19} spectrum match pretty well, the details of the line shapes do not. In fact, the details suggest that some protons have more and some less mobility than the C_{19} rotator protons. On this basis, we do not believe that the C_{30} molecules in the titania SAM undergo rotation as relatively rigid molecules as is true of the C_{19} molecules. The most obvious explanation for a gradient of mobility is the tethering at one end of the C_{30} SAM molecule.

Figure 6 shows line shapes as a function of ν_r for the silica B. Part A gives the full line shapes for ν_r values of 0, 862, 2650, and 4500 Hz and part B shows only the centerband region for 7 ν_r values from 0 to 4500 Hz. First, the cusplike shape of the nonspinning spectrum in Figure 6A again emphasizes that, in this sample, there is a wide distribution of line widths and mobilities. Second, the total intensity of the centerbands plus the spinning sidebands is a continuously increasing function of ν_r; in Figure 6A, this summed intensity constitutes about 5, 18, and 33% of the total intensity for ν_r values of 862, 2650, and 4500 Hz, respectively. Again, this behavior is more typical of a continuous distribution of mobilities, rather two or three populations, each with different, albeit uniform, mobilities. Third, the centerbands show nonsymmetric features (Figure 6B). There is an upfield shoulder at 0.9 ppm whose relative intensity, compared to the centerband maximum at 1.3 ppm, weakens slowly as ν_r increases. Also, there is a downfield "lump" centered at ~2.7 ppm. The intensity of this lump increases with ν_r. The chemical shifts of 1.3 and 0.9 ppm support the assignment of these resonances, respectively, to methylene and to methyl protons. If this is the correct assignment, then the significant relative intensity of the methyl peak suggests that, on average, the untethered ends of the molecules show the most mobility. Such a finding is consistent with other ^{13}C NMR studies of shorter, tethered chains (monofunctional silanes) on

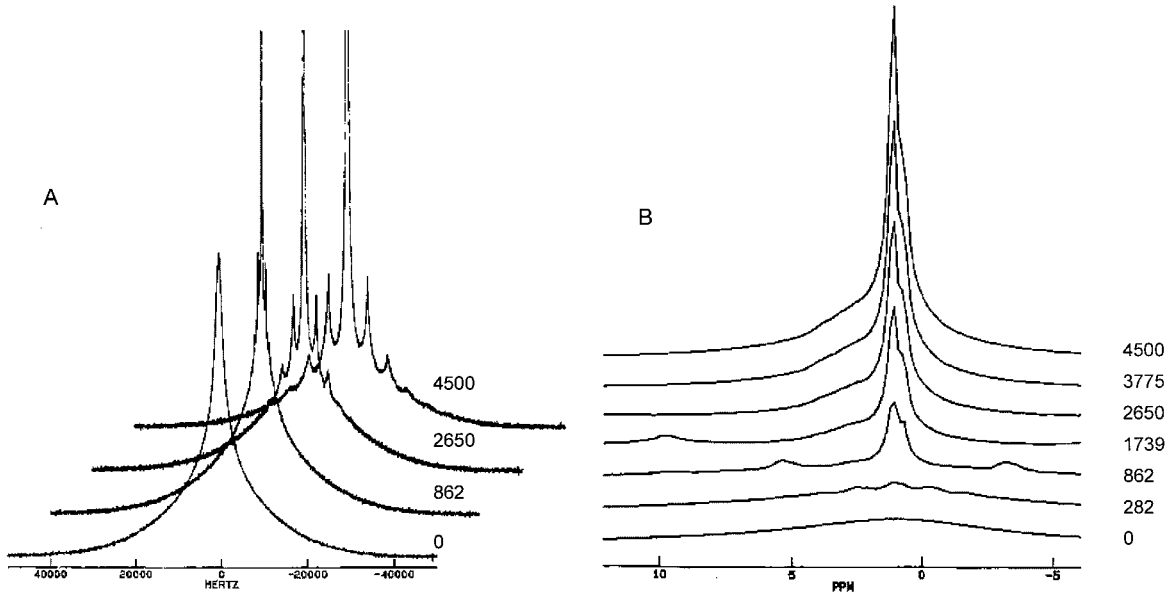

Figure 6. (A) Proton spectra, normalized to the same total intensity, of the C_{30} SAM on silica B as a function of magic angle spinning frequency (Hz). Note the development and the increased intensity of the centerband plus sidebands. This behavior is more indicative of a smooth distribution of dipolar couplings rather than a few discrete levels of dipolar coupling. (B) The centerband region only of the proton spectra corresponding to (A). Note the shoulder at 0.9 ppm (the usual chemical shift for methyl protons) and the maximum at 1.3 ppm (the usual shift for interior methylene protons). The downfield wing is not identified with the C_{30} monolayer. The strength of the 0.9 ppm shoulder suggests a preferential mobility at the free end chains.

silica surfaces.[52] The 2.7 ppm component has a chemical shift that does not correspond to any C_{30} resonance. Two centerband spectra (Supporting Information) were taken near the "null" condition at delay times of 275 and 300 ms in an inversion−recovery sequence used for the measurement of T_1^H at 200 MHz. The methylene and methyl protons in this centerband have slight differences in the times of their nulls. The protons in the broad portion of the line shape (not shown) also have a null that closely coincides with those of the 1.3 and 0.9 ppm protons. On the other hand, the protons at 2.7 ppm (Supporting Information) are still a long way from their null since they exhibit polarization levels, relative to their Boltzmann-equilibrium polarization of −0.25 and −0.18, respectively, at 275 and 300 ms. In fact, a plot (not shown) of the full T_1^H recovery shows that all the protons relax exponentially but with different T_1^H's, 580 ms for the 2.7 ppm protons and 400 ± 30 ms for the collective broad and narrow components. Thus, the polarization of the protons at 2.7 ppm does not appear to be coupled at all, even by spin diffusion, to the polarization of the C_{30} protons. This lack of polarization coupling suggests one of the following possibilities, i.e., that the 2.7 ppm protons are (a) mixed with the C_{30} SAM protons but are so highly mobile that they have almost no dipolar couplings to the C_{30} SAM protons, (b) not mixed and in the interior of the silica structure, or (c) poorly mixed and on surfaces that have very low to nonexistent C_{30} SAM coverage. While it is not critical to a discussion about the C_{30} SAM molecules to identify these extraneous protons, it would be relevant to our understanding of the extent of SAM coverage if possibility c were true. Possibility a is not likely because the intensity of the 2.7 ppm feature strongly depends on ν_r, suggesting nonnegligible dipolar couplings. On the basis of proton multiple-pulse studies[53] of unmodified silica gel, the 2.7 ppm chemical shift could conceivably arise from either adsorbed water or from hydrogen-bonded silanols. The T_1^H we observe is more consistent with T_1^H in the presence of adsorbed water as opposed to hydrogen-bonded silanols. However, the observed lack of any polarization coupling to the C_{30} SAM protons would, on a time scale of 1 s, be unexpected for adsorbed water, unless there were uncovered silica surfaces to which the water would be attracted so that these watere molecules would not spend much time in contact with the C_{30} SAM. In connection with the possibility of uncovered surfaces, it is significant that the work of Bronnimann et al. identifies isolated silanols at the silica surface as having a relatively narrow multiple-pulse resonance at 1.7 ppm. The corresponding Bloch decay resonance in our spectra should also be narrow because these protons were shown to have very weak dipolar couplings. These silanol sites should be used up when the SAM is formed. The absence of any identifiable narrow feature at 1.7 ppm in our spectra, can be taken as an indication that there are negligible uncovered surfaces present in the C_{30} SAM. Thus, while we must speculate whether the 2.7 ppm resonance arises from adsorbed water or from some protonated species internal to the silica structure, we will ignore this 2.7 ppm line in any further discussion of the C_{30} SAM protons. Incidentally, while it is difficult to see in the spectrum of Figure 5, the spectrum of the titania SAM protons does not have any significant spectral feature at 2.7 ppm; the same can be said for the zirconia SAM spectrum.

Finally, we discuss some spin diffusion experiments, mainly with an objective of addressing qualitatively the question of the uniformity of SAM density in all regions of the sample. One can select polarization on the basis of line width differences and then examine the rate at which that polarization flows out to the other proton sites via spin diffusion. We chose, in somewhat arbitrary fashion, to select polarization from narrower resonances by applying a Carr−Purcell sequence ($2\tau = 50\ \mu s$), finally using the polarization at the third echo for an initial condition in these spin diffusion experiments. We also chose ν_r to be 2650 Hz and obviously this choice has significant

(52) Sindorf, D. W.; Maciel, G. E. *J. Am. Chem. Soc.* **1983**, *105*, 1848−1851.

(53) Bronnimann, C. E.; Zeigler, R. C.; Maciel, G. E. *J. Am. Chem. Soc.* **1988**, *110*, 2023−2026.

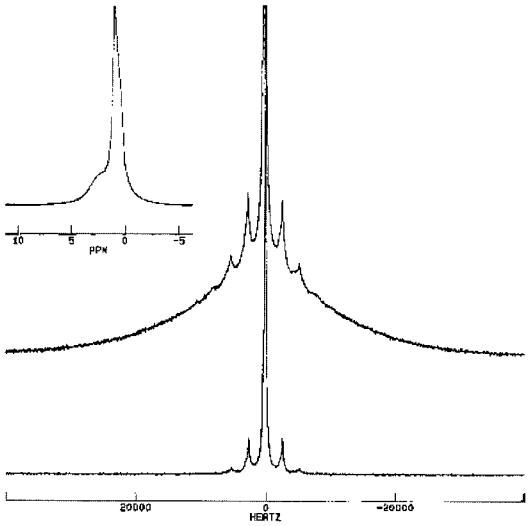

Figure 7. Proton spectra (ν_r = 2650 Hz) associated with the initial polarization selected by the spin−echo preparation in the spin diffusion measurements on the silica B sample. Bottom: spin diffusion spectrum after a short delay (t_{sd} = 0.1 ms). Middle: Boltzmann equilibrium spectrum. Inset: centerband region of lower spectrum with a 0.25 vertical scaling factor. Note the near-complete absence of the broad component in the spin diffusion spectrum as well as a nontrivial attenuation of the sideband intensities. The centerband is attenuated to a lesser degree than the sidebands; therefore, contributions to the centerband are separated into categories called "narrow" and "very narrow".

implications both for the amount of polarization that is initially obtained (see Figure 6) and most likely for the rate of spin diffusion, especially the rates involving the most mobile protons.

In Figure 7, we show the proton line shapes for the vacuum-dried silica B C_{30} SAM along with one spin diffusion spectrum taken after a short spin diffusion time, t_{sd}, of 0.1 ms. Included in Figure 7 is an inset showing the centerband region only ($\times$0.25 vertical scaling) for the latter spin diffusion line shape. The desired elimination of the broad component in this preparation is accomplished quite well. However, upon comparing the shape of the centerbands in the two spectra of Figure 7, one finds (not shown), that the centerband has changed shape in a way that suggests that there is a "very narrow", minority, high-resolution contribution to the centerband (where the 1.3 ppm and the 0.9 ppm peaks are clearly visible, but by no means fully resolved) and a majority, lower resolution, "narrow" contribution having its peak at 1.3 ppm. The latter contribution is more attenuated by the preparation. The latter contribution accounts also for most of the spinning sideband intensity provided that the sideband intensity associated with the 2.7 ppm shoulder is ignored. Thus, on the basis of the different responses, both to the T_2^H preparation and subsequently during the spin diffusion period, we separate the responses of the "narrow" and "very narrow" components of the centerband in the spin diffusion plots.

Figure 8 shows plots of the relative polarization levels, referenced to the respective Boltzmann equilibrium levels, as a function of $(t_{sd})^{1/2}$ for the various spectral components that are associated with the C_{30} SAM protons in the silica B and the titania samples, respectively. The approximate intensity fractions of the various components are given in the figure captions. Also plotted in these figures is the relative total intensity of each spin diffusion spectrum, referenced to the Boltzmann equilibrium total intensity. Plotting spin diffusion data against the square root of time produces linear initial slopes when (a) well-defined domains exist, (b) initial polarization gradients are spatially sharp at the domain boundaries, and (c) each domain has a uniform spin diffusion constant. Usually, these initial slopes give way, at longer times, to nonlinearity and a slower, monotonic approach to the polarization characteristic of internal spin equilibrium.[54] Note that the spin diffusion spectra are of rather low intensity, being only 5−10% of the Boltzmann intensities. Adjustments for T_1^H, assuming a uniform T_1^H for each component, have been made in all the data of Figure 8. The constancy of the total integrals gives good evidence that these corrections are reasonable approximations. In a system with potential inhomogeneities of coverage, the uniformity of T_1^H is not a foregone conclusion. If internal spin equilibrium is reached within the longest spin diffusion time, then the relative polarizations of all of the components should converge to the value of the relative integral. There is significant movement in that direction, but internal equilibrium is not achieved, even for t_{sd} near 300 ms. When the relevant length scale for the chemical components of a system is at most 4 nm and when, on a time scale of 300 ms, internal spin equilibrium is not achieved, one is reasonably confident that there is spatial inhomogeneity of average mobility over distances that far exceed the molecular length. But there are a few considerations, which help to clarify this statement.

As was mentioned earlier, the shape of the narrowest component of the centerband gives evidence that the methyl protons are, on average, more mobile than the methylene protons; i.e., the suggestion is strong that the free end of the C_{30} SAM molecule is most mobile. Hence, if we expect a mobility gradient to exist from the tethered end to the free end of each molecule, then it is important, in the interpretation of the spin diffusion data, to recognize the time, t^*, over which polarization could be transported through the thickness of a monolayer. We can make an estimate of the upper limit for t^* if we assume the following: (a) the maximum layer thickness is the thickness of an all-trans C_{30} segment ($\sim$3.8 nm long, assuming a projection along the chain axis of 0.127 nm/carbon), (b) the spin diffusion constant, D, is 0.4 nm^2/ms (since D for a rigid alkane lattice is expected to be $\sim$0.8 nm^2/ms,[55] the reduction by half is related to the line width for the C_{30} SAM which is, according to Figure 4, about half that of a rigid alkane), and (c) the relationship between time, t, and the mean square distance, $\langle x^2 \rangle$, that polarization will travel in a time, t, is[56]

$$\langle x^2 \rangle = 4Dt/3 \qquad (2)$$

Strictly speaking, eq 2 describes the relationship between $\langle x^2 \rangle$ and t only for those values of $\langle x^2 \rangle$ that are less than the square of the domain thickness for either the mobile or the more rigid domains. Nevertheless, substitution of $\langle x^2 \rangle = (3.8\ \text{nm})^2$ gives an approximate upper limit for t^* of 27 ms. We call this an upper limit on t^* since refinements to the approximations made in estimating t^* all result in a reduction in t^*. These refinements include the following: (a) It is possible that more than just the terminal protons are mobile (there may be a thicker layer of mobile protons, leaving a thinner layer to penetrate by spin diffusion); (b) the layer thickness may be modified both by the relaxing of the all-trans character of the chains and by any tilting of the chains with respect to the surface normals; finally, (c) the important event for spin diffusion is the propagation of

(54) Crank, J. *The Mathematics of Diffusion*; Oxford University Press: London, 1956.
(55) Vanderhart, D. L.; McFadden, G. B. *Solid State Nucl. Magn. Reson.* **1996**, *7*, 45−66.
(56) Havens, J. R.; Vanderhart, D. L. *Macromolecules* **1985**, *18*, 1663−1676.

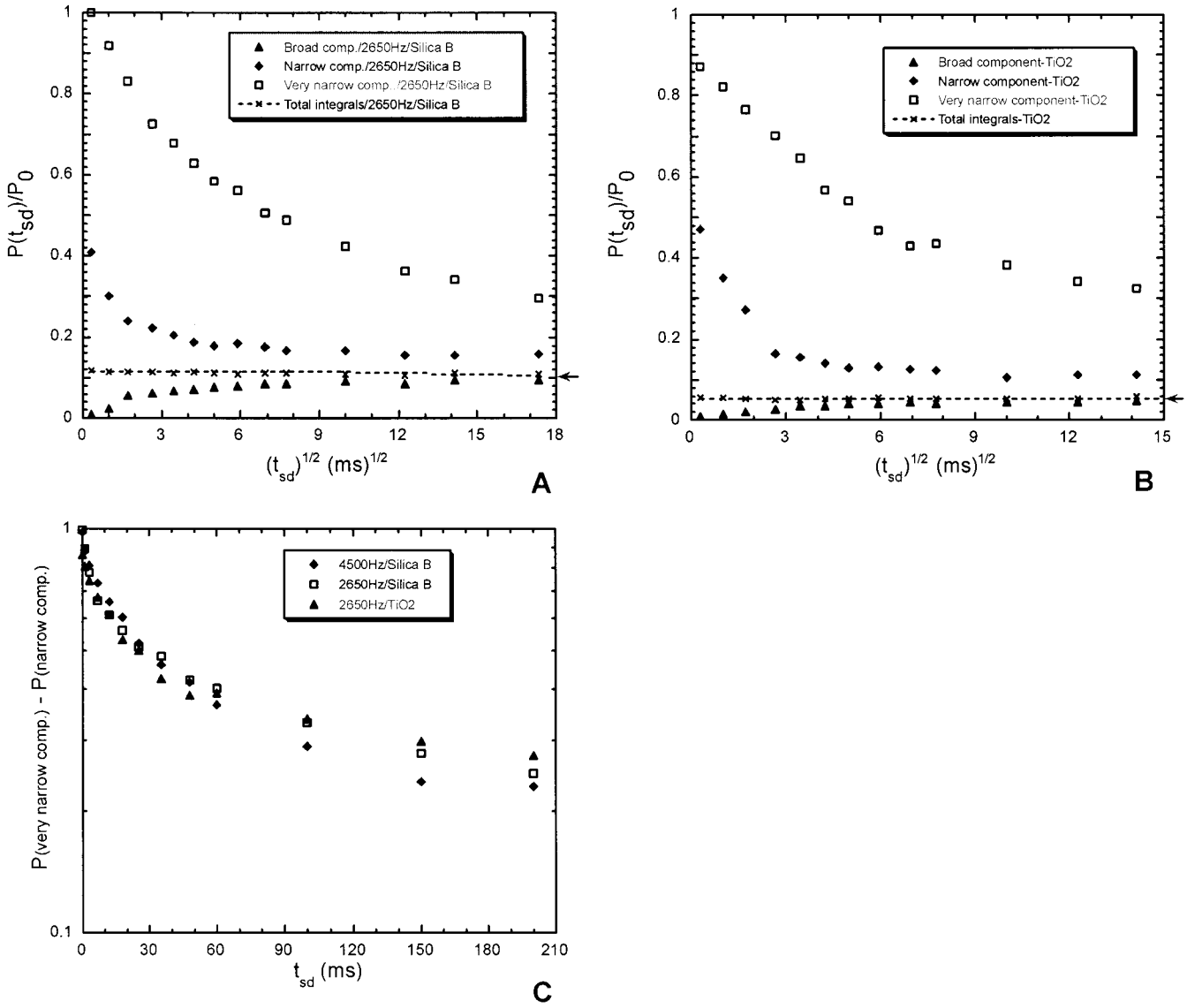

Figure 8. (A) Spin diffusion data for the C_{30} SAM protons of silica B following the polarization preparation illustrated in Figure 7. The ordinate is the ratio of the polarization of a given component during the spin diffusion experiment, relative to the Boltzmann equilibrium polarization. We associate the initial, faster decay of the "narrow" component with the movement of polarization through the thickness dimension of the monolayer. The fractions of the total C_{30} SAM proton population represented by each component are approximately 3 (very narrow), 13 (narrow), and 84% (broad). (B) Spin diffusion data, as in (A), for the C_{30} SAM protons on titania. Note the smaller total integral, relative to (A), owing to the denser packing of the SAM on titania relative to the silica B. The fractions of the total C_{30} SAM proton population represented by each component are approximately 1 (very narrow), 6 (narrow), and 93% (broad). (C) Semilogarithmic plot, combining the spin diffusion data for the "very narrow" and the "broad" components from (A) and (B). Linearity in this plot would support the hypothesis that the "very narrow" protons are both weakly and uniformly coupled to surrounding protons, which protons, in turn, would experience much stronger spin diffusion with the remaining protons. The data are not linear, hence, the alternative, namely, that there is heterogeneity of packing density, is supported.

polarization along the chain, between vicinal pairs of protons. A significant portion of the dipolar coupling is between the geminal pairs of protons in each methylene group, and if rotation of the chains is the primary type of motion occurring, it will diminish the geminal couplings more than the vicinal couplings. Hence, D may change more slowly than does the line width with the result that D for rapidly rotating chains may be closer to 0.5 or 0.6 nm^2/ms, rather than 0.4 nm^2/ms. Incidentally, the distance scale, corresponding to the 300 ms of spin diffusion data, is 12.6 nm when $D = 0.4$ nm^2/ms.

Both panels A and B in Figure 8 have similar characteristics. The polarization of the protons called "narrow" moves quickly, within ~9 ms of spin diffusion, toward the polarization of the "broad" protons; the latter representing the majority of the protons in the C_{30} SAM layer. The polarizations of these two components do not become equal, indicating that the spatial distribution of the "broad" and the "narrow" protons is not the same even on the 12-nm distance scale. In contrast to the "narrow" protons, the polarization of the "very narrow" protons decreases at a much slower pace. Again, on the 300-ms time scale, equilibrium is not achieved. A very important perspective for the data of Figure 8 comes from recognizing the relative amounts of the "narrow" and the "very narrow" protons. At 2650 Hz $= \nu_r$, our line shape analysis indicates that the "very narrow" protons make up only ~1% (titania SAM) and 3% (silica B SAM) of the total SAM protons while the "narrow" protons constitute about 6 and 13%, respectively. These relative amounts and the fact that the "very narrow" protons undergo a larger change in polarization than do the "narrow" protons implies that the growth of the "broad" proton polarization with t_{sd} can be traced to substantial spin diffusion contributions from both the "narrow" and the "very narrow" protons.

In panels A and B of Figure 8, we interpret the 9-ms time scale, mentioned in the preceding paragraph, to be the time scale during which polarization, initially located in the mobile elevations of a layer, moves through the thickness of the layer toward the substrate surface. Clearly, 9 ms is not the 27 ms we had estimated for t^*; however, since that was an upper limit, the 9 ms is not beyond possibility. Note that these "narrow" protons are the major contributors to the centerband and spinning sidebands. So the picture that emerges is that, at $\nu_r = 2650$ Hz, four to eight methylene protons, on average, near the free ends of each C_{30} chain will contribute to the "narrow" component and over the first, say, 20 ms of spin diffusion, polarization equilibrates throughout the thickness of most layers.

Interpretation of the spin diffusion behavior of the "very narrow" proton polarization is more complicated. (The high mobility of these protons suggests that their attached ^{13}C nuclei are probably responsible for some of the narrowest contributions to the methyl and α-methylene carbon resonances.) Since these protons are so mobile, we must entertain the possibility that the dipolar coupling of these protons to other protons is so weak that the rate-limiting step in spin equilibration is polarization exchange between a "very narrow" proton and a "broad" (or even a "narrow") proton. To test the foregoing hypothesis, we set up a very crude model in which we suppose that (a) the polarization exchange rate, R_x, describing polarization exchange between a "very narrow" and a "broad" proton were uniform for all "very narrow" protons and (b) spin diffusion over times, $1/R_x$, is extensive enough to equilibrate polarization among the "broad" protons. We further assume that the following equation applies:

$$dP_{VN}/dt_{sd} = -R_x(P_{VN} - P_B) \quad (3)$$

where P_{VN} and P_B are, respectively, the polarizations of the "very narrow" and the "broad" protons after these polarizations have been corrected for T_1^H effects. Using the further approximation that P_B is a constant and not the weak function of t_{sd} that it is, eq 3 can be integrated to give the equation

$$[P_{VN}(t_{sd}) - P_B(t_{sd})]/[P_{VN}(t_{sd} = 0) - P_B(t_{sd}=0)] = \exp(-R_x t_{sd}) \quad (4)$$

In Figure 8C, the quantity $[P_{VN}(t_{sd}) - P_B(t_{sd})]$, taken from the data of Figure 8A and B, is plotted versus t_{sd} in a semilog plot. It is clear that eq 4 is *not* obeyed; i.e., this plot is definitely not linear, not even in the interval from 15 to 300 ms where the changes in $P_B(t_{sd})$ are very minor. Thus, we conclude that the model of uniform, very slow polarization exchange rates involving the "very narrow" protons does not apply.

The foregoing result, taken together with the fact that the "narrow" and the "broad" proton polarizations do not fully equilibrate on the 300-ms time scale, suggests that there is heterogeneity in the density of coverage over dimensions of at least 20 nm, a distance about twice the spin diffusion distance corresponding to $t_{sd} = 300$ ms. We use the factor of 2 by assuming that any domain would be surrounded on at least two sides by domains of contrasting mobility. Recall that a large portion of the changes (Figure 8A and B) in the "narrow" proton polarization has been assigned to spin equilibration with "broad" proton polarization via spin diffusion along the thickness dimension of the SAM. Then it is perhaps not so clear why the "narrow" and the "broad" polarizations do not fully equilibrate to the same average polarization since the associated protons share the same molecule. Incomplete equilibration can happen when, over domains exceeding 20 nm, the fraction of C_{30} protons in the "broad" versus the "narrow" categories varies, i.e., when there is greater or lesser average mobility over these dimensions. That is the qualitative model we are suggesting. It follows that there might well be domains on the scale of at least 20 nm that lack any "very narrow" protons.

To summarize the proton results, the C_{30} SAM line shapes show extensive motional averaging to give a line width similar to that of the C_{19} rotator phase. A greater heterogeneity of mobility, relative to the mobility of C_{19}, is present in the C_{30} SAMs; hence, the rotator-phase model for the SAMs is too simplistic and is only supported in the most qualitative sense. As to the uniformity of the density of chain packing in the SAMs, spin diffusion experiments indicate that there is considerable variation in the average mobility and, by implication, in packing density, on a scale of at least 20 nm.

The fast overall motions of the chains are probably important to the functioning of these SAMs as shape-selective surfaces for chemical separation. It is less clear what the role of heterogeneity in packing density is and how that relates to chromatographic separation. One might surmise that if heterogeneity in packing density arose mainly because of the nonidealities of carrying out a reaction in labyrinthine internal pores, each particle might contain similar distributions of packing density and mobility. If this were so, then one's ability to tailor selectivity might be compromised; however, one would not necessarily see evidence of the heterogeneity in terms of broader elution peaks. At the same time, if heterogeneous coverage is related to the path length of the pore from the nearest entry point on the particle, then variations in particle size could conceivably lead to broader elution peaks. In other words, one might sharpen elution peaks by making particle size more homogeneous despite heterogeneous SAM density in the particle interior.

Liquid Chromatography Studies. To assess shape selectivity properties of reversed-phase LC columns, it is useful to evaluate the selectivity coefficient for tetrabenzonaphthalene (TBN) and benzo[*a*]pyrene (BaP). These solutes are included in SRM 869a, a three-component column selectivity test mixture that was designed to classify commercial C_{18} columns for the separation of PAHs.[57,58] Significant differences have been reported in $\alpha_{TBN/BaP}$ values determined among monomeric and polymeric C_{18} phases.[32] For monomeric C_{18} columns $\alpha_{TBN/BaP}$ values are greater than 1.7, and for polymeric C_{18} phases $\alpha_{TBN/BaP}$ is less than 1.0. SRM 869a was separated on the C_{30} self-assembled monolayer columns in order to assess the polymeric nature of the phase and to evaluate the efficiency of the new materials.

Table 2 summarizes $\alpha_{TBN/BaP}$ values, plate numbers (N), and asymmetry factors (A). Column efficiencies for the various C_{30} phases are much lower than for monomeric C_{18} phases, and peak asymmetries for TBN range from 1.3 to 1.7. Reduced efficiency and peak asymmetry has been reported for densely bonded phases resulting from the self-assembled monolayer synthesis.[32] Mass-transfer kinetics may also be affected by the long alkyl chains. Enhanced shape selectivity properties are indicated for the C_{30} phases by the $\alpha_{TBN/BaP}$ values, which are less than 0.7 and representative of polymeric-like surface modification. A similar selectivity coefficient ($\alpha_{TBN/BaP} = 0.6$) was also found by Ellwanger et al. for polymeric C_{18}-modified TiO_2.[29] The $\alpha_{TBN/BaP}$ values determined for the C_{30} SAMs correlate well with the trans/trans-gauche ratio determined by ^{13}C solid-state NMR measurements (Figure 1). The largest

(57) Sander, L. C.; Wise, S. A. *LC-GC* **1990**, *8*, 378−390.
(58) Sander, L. C.; Wise, S. A. *Certificate of Analysis, Standard Reference Material 869, Column Selectivity Test Mixture*; NIST: Gaithersburg, MD, 1990.

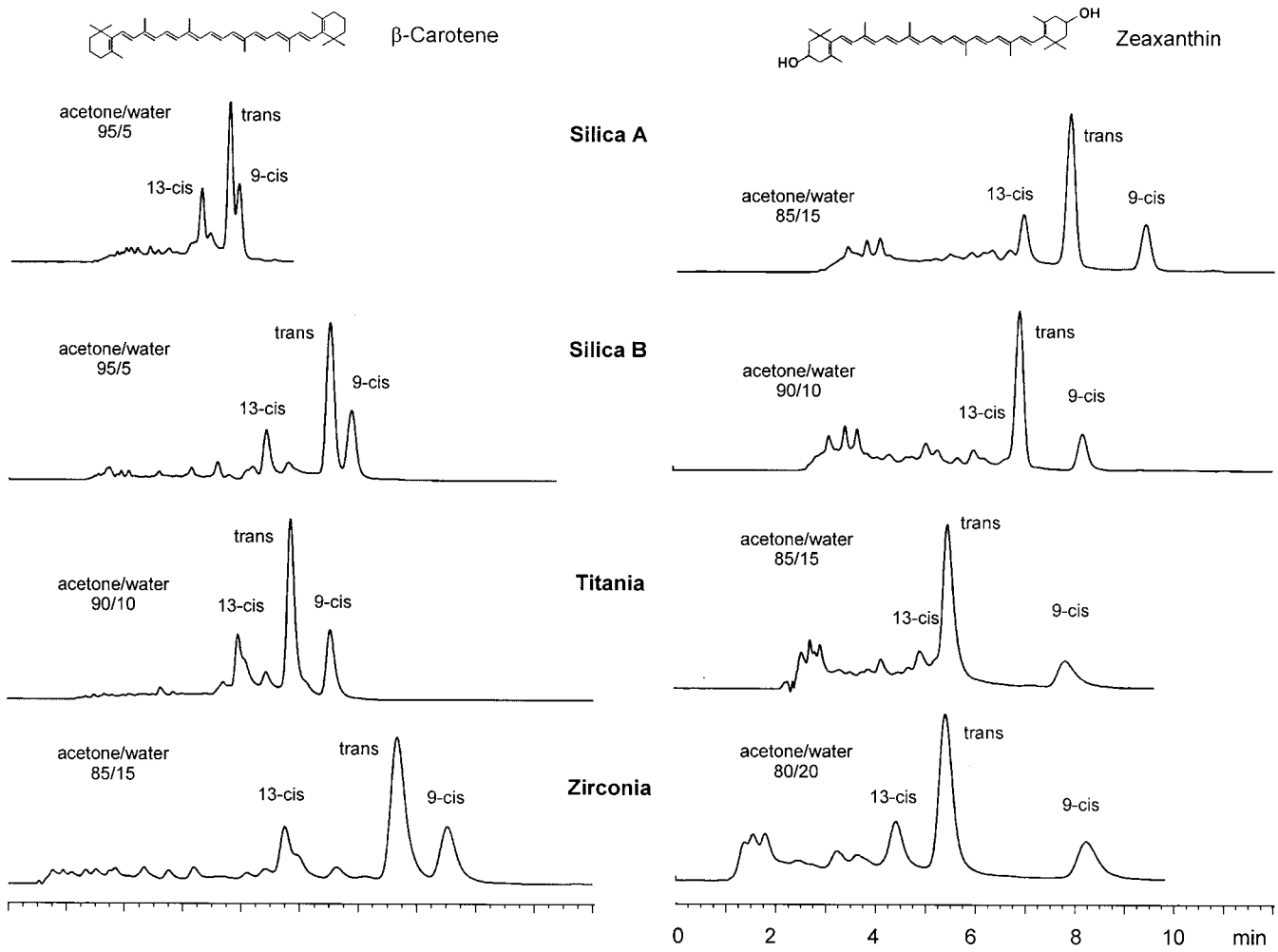

Figure 9. Separations of β-carotene and zeaxanthin isomers on C_{30} self-assembled monolayers.

selectivity factor ($\alpha_{TBN/BaP} = 0.64$) was observed for the silica A C_{30} material. This stationary phase possesses the highest fraction of gauche conformations and therefore has the lowest shape selectivity properties among all the columns. Similar correlations can be made for the other materials.

Carotenoids are nutrients found naturally in a variety of sources. This class of compounds is receiving increasing attention due to their antioxidant properties and their role in vitamin A activity, as well as possible health benefits in cancer prevention and therapy. Carotenoids occur in many fruits, in vegetables, and in animal tissue. Due to the polyene system, many geometric isomers are formed under influence of light, heat, or oxygen. Because the biological activity varies among the isomers, it is therefore important to separate the individual isomers. It has been shown that the C_{30} system is superior to C_{18} phases for separating carotenoid isomers.[9] Separations of β-carotene and zeaxanthin isomers on the C_{30} self-assembled monolayers are illustrated in Figure 9; for separations of tocopherols see Supporting Information.

Selectivity differences can be observed among the four columns for β-carotene isomers. Complete separation of 13-cis, trans, and 9-cis isomers was achieved with the C_{30} phases on silica B, titania, and zirconia. In contrast, poor separation of these isomers resulted from the C_{30} bonded silica A, which has a lower alkyl chain order (Figure 1). The best selectivity toward the β-carotene isomers is exhibited by the titania and zirconia C_{30} phases. This can be seen in the higher $\alpha_{9-cis/trans}$ value on the titania and zirconia C_{30} phases (see Supporting Information). The information provided by SRM 869 on shape selectivity and the NMR results on alkyl chain order are also indicative of column selectivity toward β-carotene isomers. This confirms the findings of Lesellier et al., who compared a series of C_{18} phases with regard to selectivity for SRM 869 and carotenoid isomers.[59] Although selectivities between 9-cis and trans β-carotene could not be determined for most of the investigated C_{18} columns because these isomers were not resolved, a similar trend is found. Lower $\alpha_{TBN/BaP}$ values correspond with better separation of β-carotene isomers.

The higher chain order (hence, the enhanced shape selectivity) for the titania and zirconia SAMs can probably be attributed to the more ordered, crystal-like character of these inorganic supports compared to the rather amorphous nature of silica. SAM formation should be facilitated on more homogeneous, flat surfaces with more regular arrays of binding sites.

For zeaxanthin isomers (Figure 9) shape selectivity alone cannot account for the observed retention behavior. All four columns separate the three isomers (9-cis, trans, 13-cis) well; however, the highest $\alpha_{9-cis/trans}$ values are found for zirconia- and titania-based C_{30} phases (see Supporting Information). Remarkably, the lowest covered C_{30} phase (silica A) gives the same separation results as the C_{30} material on silica B (higher alkyl chain order). It appears that, for these polar isomers, surface hydroxyl group activity plays a more important role than chain order.[59] The influence of surface silanols for separations of polar carotenoids has been observed between end-capped and non-end-capped C_{30} phases.[9]

(59) Lesellier, E.; Tchapla, A.; Krstulovic, A. M. *J. Chromatogr.* **1993**, *645*, 29−39.

Conclusions

C_{30} self-assembled monolayers have been prepared on three inorganic oxides: silica, titania, and zirconia. Solid-state NMR spectroscopy revealed considerable differences in average chain order from sample to sample. Also, there was heterogeneity of chain order within each of the samples; i.e., the density of coverage is not uniform. Certain correspondences between NMR data from the C_{19} rotator phase and the more ordered regions of the C_{30} SAMs, suggest that diffusional chain rotation may capture at least an important facet of the motion in the more ordered C_{30} regions. While diffusional rotation is not particularly consistent with a mobility gradient along the chain axis, it is consistent with both the presence of fast, large-amplitude motions and the preservation of all-trans interior-methylene conformations. The fact that the reactant molecules, which form these C_{30} phases, consist of chains with a distribution of chain lengths adds complexity to the interpretation of the data. No doubt, this distribution also adds texture to the surface of the C_{30} phase as shown by AFM images. LC data from separations of shape-selective compounds are in agreement with the NMR results. Molecular shape recognition in separations of PAHs and nonpolar carotenoid isomers correlates well with the data on alkyl chain order. For polar solutes such as tocopherols and xanthophylls, chain order is not the major criterion for the observed retention behavior. Due to their higher molecular shape recognition capabilities, the titania and zirconia reversed-phase materials provide an alternative to silica for separations of carotenoids.

Acknowledgment. We are thankful to Bischoff Chromatography GmbH (Leonberg, Germany), Merck KGaA (Darmstadt, Germany), Sachtleben AG (Duisburg, Germany), and ZirChrom Separations Inc. (Anoka, MN) for the donation of the base materials. M.P. thanks the Alexander-von-Humboldt foundation (Bonn, Germany) for a Feodor-Lynen fellowship and Wolfgang Haller (NIST) for helpful discussions.

Supporting Information Available: Table of phase selectivities, plot of two-proton centerband-only line shapes for the C_{30} SAM protons, and separation of tocopherol isomers on C_{30} SAMs (PDF). This material is available free of charge via the Internet at http://pubs.acs.org.

JA993705D